Ecological Indicators 110 (2020) 105939

Contents lists available at ScienceDirect

Ecological Indicators

journal homepage: www.elsevier.com/locate/ecolind

Original Articles

Variation trend of global soil moisture and its cause analysis

Yuanhong Deng[a,b,c], Shijie Wang[a,d], Xiaoyong Bai[a,e,f,*], Guangjie Luo[f], Luhua Wu[a,c], Yue Cao[a,c], Huiwen Li[a,c], Chaojun Li[a,g], Yujie Yang[a,g], Zeyin Hu[a,b,c], Shiqi Tian[a,g]

[a] State Key Laboratory of Environmental Geochemistry, Institute of Geochemistry, Chinese Academy of Sciences, Guiyang 550081, China
[b] Center for Lunar and Planetary Sciences, Institute of Geochemistry, Chinese Academy of Sciences, Guiyang 550081, China
[c] University of Chinese Academy of Sciences, Beijing 100049, China
[d] Puding Karst Ecosystem Observation and Research Station, Chinese Academy of Sciences, Anshun 562100, China
[e] CAS Center for Excellence in Quaternary Science and Global Change, Xi'an 710061, China
[f] Guizhou Provincial Key Laboratory of Geographic State Monitoring of Watershed, Guizhou Education University, Guiyang 550018, China
[g] School of Geography and Environmental Sciences, Guizhou Normal University, Guiyang 550001, China

ARTICLE INFO

Keywords:
Soil moisture
NDVI
Precipitation
Drying
Global
Remote sensing

ABSTRACT

Soil moisture (SM) is a comprehensive variable of terrestrial ecosystems. However, the global SM trend in recent decades and the future is uncertain, and the main factors causing soil drying and wetting are not fully understood. This study using Extended Triple Collation, Mann-Kendall test, Theil-Sen estimate, Hurst exponent, Ensemble Empirical Mode Decomposition and pertinent methods found that 1) at the pixel scale, the long-term daily SM data from ERA-Interim was closest to the true SM compared with ESA CCI and GLDAS; 2) the global average SM in 1979–2017 decreased remarkably and the declining trend accelerated in 2001–2017; 3) soil drying was observed in seven major land covers; among which, urban area has the largest area proportion of soil drying, about 80%; 4) the strong persistence of SM trend indicates that the global future soil will continuously be dominated by a drying trend; 5) overall, 65.1% of the global soil drying trend was attributed to temperature rising, whereas 82% of the wetting trend was affected by the combined action of temperature, precipitation, and NDVI. Under global warming, the soil drying area expanded at a rate of 1% yr^{-1} in 1979–2017 and the global SM will keep diminishing in the next years, which may increase the risks of extreme heatwaves, water resources shortage, land degradation, and other eco-environmental problems.

1. Introduction

As a critical comprehensive variable of terrestrial ecosystems, soil moisture (SM) is the carrier of soil material transport (Legates et al., 2011), and sufficient SM is the basic condition for plant growth (Padilla and Pugnaire, 2007); additionally, SM affects water cycle and has mutual feedback effects with climate (Koster et al., 2003; Taylor et al., 2012; Deng et al., 2018). Therefore, the changing trend of SM should be studied for the soil water resources, hydrological processes, climate prediction, especially under global warming (Cai et al., 2009; Valdes et al., 2015; Deng et al., 2019). Currently, some progresses have been achieved in this field on a global scale. However, divergence exists in their conclusions due to different data and study periods. Sheffield and Wood (2008) found that global SM experienced a wetting trend from 1950 to 2000 by using data from a land surface model; Albergel et al. (2013) observed that the SM from ESA CCI and ERA-Land was dominated by reduction from 1988 to 2010, which was different from the result of MERRA-Land product that the areas where the global SM changes significantly was mainly wetting in the same period. Moreover, the future trend of global SM requires further understanding, which plays an important role in the early warning of future agricultural disasters and climate change.

Currently, SM data are available from diverse sources. Among them, the multi-satellite SM from ESA CCI, the simulated SM from GLDAS land surface models, and ERA-Interim reanalysis data, after validated by many scholars based on in-situ observational data (Berg, et al., 2005), are widely applied in spatial–temporal variations of SM, hydrometeorology, numerical simulation and other fields (Albergel et al., 2012a, 2012b; Zhang et al., 2008). The verification from 197 stations worldwide, such as the United States, Australia, and China, revealed that time series of SM from ERA-Interim and ESA CCI well captured the changes of in-situ SM from 2007 to 2010, with their average correlation

* Corresponding author at: State Key Laboratory of Environmental Geochemistry, Institute of Geochemistry, Chinese Academy of Sciences. 99 Lincheng West Road, Guiyang 550081, Guizhou Province, China.
E-mail address: baixiaoyong@vip.skleg.cn (X. Bai).

https://doi.org/10.1016/j.ecolind.2019.105939
Received 26 April 2019; Received in revised form 10 November 2019; Accepted 13 November 2019

coefficients of 0.68 and 0.60, respectively (Albergel et al., 2013). Zeng et al. (2015) found that compared with ERA-Interim, the SM from ESA CCI in the Qinghai-Tibet Plateau of China had a stronger correlation with SM from stations; and, Kim et al. (2018) found that the average correlation coefficient between SM from GLDAS-Noah and global in-situ observations was 0.73, which performed better than ASCAT and AMSR2; Dorigo et al. (2012) pointed out that the dominant trends of SM from ESA CCI, GLDAS-Noah, and ERA-Interim in 1988–2010 were consistent, that is, global soil was drying; however, spatial distributions of their trends differ, which makes it essential to assess the reliability of SM products. Many studies evaluate non-measured products at pixel scale by using limited in-situ observations and then select better products to study SM further. Nonetheless, the in-situ SM is not necessarily the "true" SM, and the scale differences between the site and the pixel affect the evaluation results; more importantly, due to short observational time, the SM data from stations is usually applicable to the verification for short-term SM products, which fails to meet the trend analysis demands for reliable long-term sequence data. The Triple collation (TC), firstly introduced into the assessment of SM products from remote sensing by Scipal et al. (2008), can solve the above problems and get three sets of data error estimates simultaneously. The original TC is a robust, objective, and promising evaluation method (Scipal et al., 2010), but it cannot estimate the correlation coefficients between three datasets and the unknown true SM, which is critical to the reliability of trend analysis of SM change; besides, TC is rarely applied to assess SM products from land surface model and reanalysis. Therefore, the new improved extended TC (ETC) can be used to evaluate multi-source SM products (Su et al., 2014; McColl et al., 2014; Chen et al., 2018a).

The spatiotemporal variability of SM is influenced by many factors, such as precipitation, temperature, land use and vegetation (Cheng and Huang, 2016; Wang et al., 2013). The spatial distribution of SM and its hydraulic properties are different under various land use types. Chen et al., (2009) found that SM contents of forest, shrub, and grassland were 30.5%, 20.1%, and 10.2%, respectively, higher than that of bare area. Precipitation is an important income of SM (Wu et al., 2002), and temperature affects SM through the balance of land surface energy budget. The rising of temperature increases land surface evapotranspiration and then reduces SM (Cheng and Huang, 2016). Vegetation has the ecological functions of storing and conserving water but can also absorb and consume plenty of soil water (Li, 2001; English et al., 2005; Wang et al. 2018). The effects of various factors on SM have been studied, but the main factors affecting the drying and wetting trends of global SM in previous studies are lacking.

Thus, this study aims to 1) apply ETC to evaluate the applicability of three SM products; 2) choose the best SM product to reveal the trend characteristics of global SM; 3) analyze global SM trend after the study period; and 4) explore the major causes affecting the trend of SM and the impacts of soil drying.

2. Materials and methods

2.1. Data and preparing

ESA CCI SM product (http://www.esa-cci.org/) is obtained from European Space Agency (ESA) in the implementation of the Global Basic Climate Change Initiative (CCI) by combining SM products from active and passive microwave (Dorigo et al., 2015). It contains three products, namely, the Passive microwave product by merging four passive microwave SM data sets with the AMSR-E SM as the reference, the Active microwave product by merging two active microwave SM data sets with ASCAT SM as the reference and the Combined product by merging the Passive and Active products. Previous studies have found that except for ASCAT, the Combined product of ESA CCI is better than any microwave products it has merged (Dorigo et al., 2015). Therefore, the Combined product is used in this study, which covers a long period (Table 1). The SM depth detected by the product is ~ 5 cm.

ERA-Interim SM product (https://www.ecmwf.int/) is created by the European Centre for Medium-Range Weather Forecasts (ECMWF) by using TESSEL land surface model and 4D-VAR assimilation algorithm (Dee et al., 2011). Compared with the previous ERA-40, ERA-Interim has shown great advantages in global atmospheric quality, moisture, energy, and angular momentum budget, and its SM product has made many improvements in time coverage, prediction model and error correction. Meanwhile, the product contains four layers of SM, and their depths are 0–7, 7–28, 28–100 and 100–289 cm.

GLDAS, Global Land Surface Data Assimilation System, is developed jointly by the Goddard Space Flight Center of NASA and the National Center for Environmental Forecasting of the United States Oceanic and Atmospheric Administration (https://disc.gsfc.nasa.gov/). Based on surface observations and satellite remote sensing monitoring data, its four land surface process models including Noah have simulated SM products with various spatiotemporal resolutions (Rodell et al., 2004). This study adopted SM product from Noah (version 2.7.1) model, which contains four layers of SM data with their depths of 0–10, 10–40, 40–100 and 100–200 cm, respectively. The product uses the SM content of the average layer, unit: kg/m^2.

Global land cover dataset is provided by ESA CCI (http://maps.elie.ucl.ac.be/CCI/viewer/download.php), which contains 37 types of land cover (ESA, 2018; Li et al., 2018). *Precipitation and Temperature data* (http://www.cru.uea.ac.uk/data) are reconstructed by the Climate Research Institute of the University of East Anglia (CRU) by integrating several well-known databases. It is a complete, high-resolution, non-missing global grid dataset (Harris et al., 2014). *GIMMS NDVI3g* (https://ecocast.arc.nasa.gov/data/pub/gimms/) is produced by NASA's Global Inventory Modeling and Mapping Studies (GIMMS) team based on the Advanced Very High Resolution Radiometer (AVHRR) images on NOAA series satellites, which are processed with strict quality control to generate maximum synthetic products (Tian et al., 2015).

An overview of the above data is shown in Table 1. The major properties of surface SM and deeper SM are similar (Brocca et al., 2011; McColl et al., 2017). Therefore, ERA-Interim SM at 7 cm and GLDAS SM at 0–10 cm were adopted in this study. To compare with other SM products, the SM unit, kg/m^2, of GLDAS was converted into m^3/m^3, soil volumetric moisture content. Then, three SM products were processed into daily data at 1-degree resolution; and, to ensure the reliability of the results, the ETC method was conducted in areas where the correlation coefficients among three SM daily data in 1979–2016 were significantly over zero (P value $\geq$ 0.05). Meanwhile, based on the 1992–2015 global land cover data, the perennial snow-covered areas of glaciers were masked out; following IPCC land categories, land cover types were merged into seven major types: Agriculture, Forest, Grassland, Shrubland, Sparse vegetation, Urban and Bare area.

2.2. Methods

The improved ETC method based on TC requires three sets of spatiotemporal matching and independent datasets and has the same conditions as the TC method (McColl et al., 2014). The detailed algorithms can be found in Text S1. To avoid the numerical problems in the error estimation process, the sample number of each independent dataset in this paper is over 100.

Mann-Kendall (MK) test is a non-parametric statistical test to detect change trend and mutation point of time series (Yue et al., 2002), which is generally combined with Theil-Sen trend analysis to analyze the changing trend of research elements (Fernandes and Leblanc, 2005). When the time series has a changing trend after identified by the MK test, the Theil-Sen slope is estimated (Sen, 1968).

Hurst exponent can be used to characterize the long-range dependence of time series of research elements quantitatively. By the Hurst value, whether the SM trend is persistent or not can be judged, which

Table 1
Overview of datasets used in this study.

Data	Data type	Spatial coverage	Temporal coverage	Spatial resolution	Temporal resolution
ERA-Interim	Reanalysis	−90–90°N, 0–359.5°E	1979–Present	0.5°	1 d
ESA CCI	Remote sensing	−89.875–89.875°N, −179.875–179.875°E	1978–2016	0.25°	1 d
GLDAS	Land model	−60–90°N, −180–180°E	1979–Present	1°	3 h
Land cover	Remote sensing	−90–90°N, −180–180°E	1992–2015	300 m	Annual
Precipitation and temperature	Reanalysis	−89.75–89.75°N, −179.75–179.75°E	1901–2016	0.5°	Monthly
GIMMS NDVI3g	Remote sensing	−90–90°N, −180–180°E	1981.7–2015.12	8 km	15 d

reflects the trend of SM in the future. 1) Hurst ∈ (0, 0.5) indicates that SM time series has anti-persistence, and the future trend is contrary to that of the current research period, and the closer to 0, the stronger the anti-persistence; 2) Hurst = 0.5 indicates that SM time series does not have long-range dependence and is a random sequence; 3) Hurst ∈ (0.5, 1), the SM time series is persistent, and its future trend is consistent with the past, and the closer to 1, the stronger the persistence (Wu et al., 2017). V-statistics can test the stability of Hurst results and quantitatively describe the stable and lasting time of the time series in the future. Detailed calculation methods can be referred to Text S1.

EEMD (Ensemble Empirical Mode Decomposition) is a signal analysis method improved by Huang Pi's team based on Empirical Mode Decomposition. Compared with wavelet analysis, it does not need any basis function (Qin et al., 2012). A non-stationary time series can obtain intrinsic mode functions with different scales and a residual term representing the overall trend of the original signal by adopting EEMD decomposition. According to Huang et al. (1998), the perturbed white noise with the signal-to-noise ratio of 0.2 to the original signal was used in the present study, and the number of samples was 100. The detailed steps can be found in Text S1.

3. Results

3.1. ETC results

In Fig. 1a-c, the correlation between ERA-Interim SM product and the unknown true SM is the strongest, followed by ESA CCI, and SM simulated by GLDAS performs the worst. The statistics show that the global average R^2 values of the three products are 0.56, 0.52, and 0.16, respectively, i.e., the global average correlation coefficients are 0.748, 0.721, and 0.4. Meanwhile, the SM products from three different sources are poor in high latitude land areas (near 60 °N) of the northern hemisphere; and, the correlation of ESA CCI in the Sahara Desert area also performs poorly. The RMSE results are consistent with those of R^2 (Fig. 1d-f). Concretely, ERA-Interim SM has the highest accuracy, with its RMSE ranging from 0 to 0.058 m^3/m^3 and the average RMSE of 0.021 m^3/m^3, followed by ESA CCI with RMSE varying between 0–0.077 m^3/m^3 and the average RMSE of 0.033 m^3/m^3. RMSE of GLDAS is between 0–0.103 m^3/m^3 with the average RMSE of 0.038 m^3/m^3. In summary, ERA-Interim SM in regions meeting ETC conditions is closest to the unknown true SM in 1979–2016. Therefore, combined with its good performance validated by the global in-situ data in previous research (Albergel et al., 2013), the SM product from ERA-Interim is used later to analyze global soil moisture trend, causes and impacts of soil drying, and the study period is 1979–2017.

3.2. Trend characteristics of soil moisture

3.2.1. Global soil moisture dynamic trend and its spatial distribution

The global average annual SM in 1979–2017 ranged from 0.265 to 0.275 m^3/m^3 with an average of 0.271 m^3/m^3. In Fig. 2, the MK test demonstrates that the global SM declined from 1979 to 2017 with the trend changing suddenly in 2001; SM decreased significantly during 2001–2017 (the UF curve exceeding the 95% confidence interval) with the rate of -0.126×10^{-3} m^3/m^3 yr^{-1} being twice that of 1979–2000 (-0.046×10^{-3} m^3/m^3 yr^{-1}); after 2001, global SM was lower than the multi-year average, namely, the global soil was in an overall dry status. Integrated with the MK trend test, the Theil-Sen slope of the global average SM is estimated to be -0.145×10^{-3} m^3/m^3 yr^{-1} with the 95% confidence interval from -0.174 to -0.116×10^{-3} m^3/m^3 yr^{-1}, and the linear regression shows that the global SM changing rate was -0.2×10^{-3} m^3/m^3 yr^{-1} with its determination coefficient over 0.69 in the study period.

Regional differences exist in the spatial distribution of the SM trend detected by the MK test (Fig. 2c1). But, the area with SM reducing accounts for 67.96%, indicating that the global soil was spatially dominated by a drying trend in 1979–2017; and, 35.66% of the global SM decreased significantly, mainly distributed in eastern China, Mongolia, southern Russia, eastern European Plain, north-central Africa, the United States, and eastern Brazil, which is consistent with the conclusion of Dorigo et al. (2012). The African Sahel with serious soil drying problem in previous studies is also observed in our study (Alonge et al., 2007; Rodriguez-Fonseca et al., 2015). Meanwhile, SM in 12.76% of the global area significantly elevated, located in India, Bangladesh, and other South Asia areas as well as the East African Plateau and the northwest of South America. The spatial pattern of Theil-Sen slope is similar to that of the Z value from the MK test and it is found that the average rate of soil drying area (-0.373×10^{-3} m^3/m^3 yr^{-1}) is faster than that of soil wetting area (0.257×10^{-3} m^3/m^3 yr^{-1}). By Z value and the spatial mean of global SM Theil-Sen slope, the Theil-Sen slope was divided into five grades (Table S1) and the SM drying rate in 32.39% of the globe covered with SM data was significantly faster than the global average level.

3.2.2. Soil moisture trends under different land covers

The multi-year average SM values of global Agriculture, Forest, Grassland, Shrubland, Sparse vegetation, Urban area, and Bare area are 0.257, 0.301, 0.253, 0.242, 0.266, 0.256 and 0.166 m^3/m^3, respectively. In Fig. 3a-g, all the land covers showed declining trends in SM from 1979 to 2017. SM in Bare area decreased fastest with its rate of -0.41×10^{-3} m^3/m^3 yr^{-1}, followed by Agriculture, Urban area, Grassland, Shrubland, while SM in Forest and Sparse vegetation reduced the slowest with their rates of -0.1×10^{-3} and -0.08×10^{-3} m^3/m^3 yr^{-1}, respectively. Compared with Bare area, Forest and other vegetation-covered land covers have higher SM values and slower rates of SM reduction, and SM in Shrubland and Grassland decreases faster than SM in Forest. It may be because vegetation has the function of water storage and water conservation (Zhang et al., 2016) and the function varies with the vegetation types. Moreover, the differences in SM change rates among Forest, Agriculture and Urban area suggest that

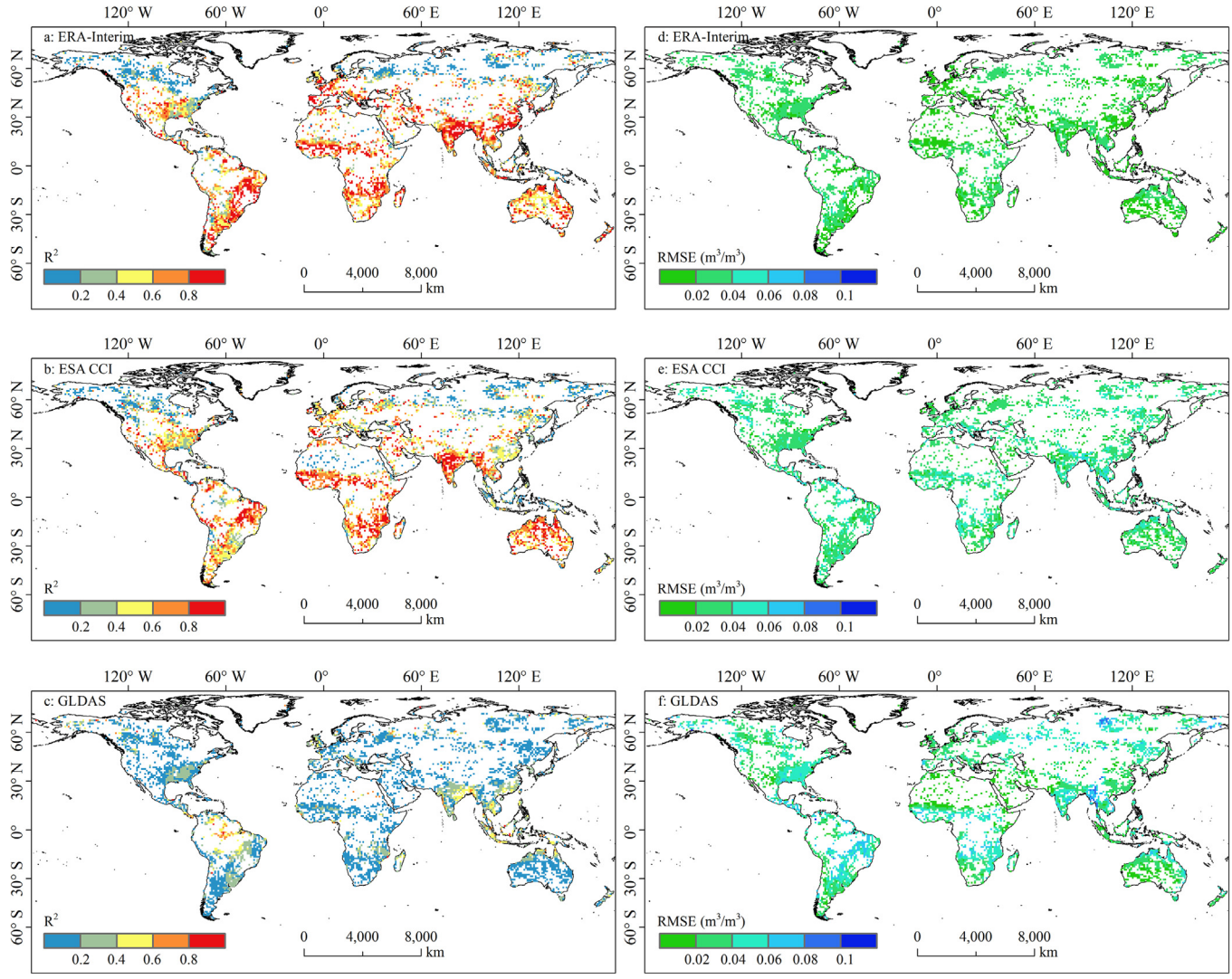

Fig. 1. Spatial distributions for correlation coefficient' square (a-c) and RMSE (d-f) of SM products from ERA-Interim, ESA CCI, and GLDAS with unknown true SM. Blank areas mean no data, e.g., ESC CCI has no SM data in tropical rain forest areas such as Congo Basin in Africa, or mean that ETC conditions are not satisfied in these places.

intensive human activities may accelerate the soil drying trend. Especially, in Fig. 3h, the areas with negative Theil-Sen slope in seven land covers are over 50% with Urban area largest approaching 80%. Hence, soil drying trend occupied a spatial dominant position in these land covers. In addition, on the global scale, the soil drying areas mainly come from Forest, Grassland and Bare area and the soil wetting areas are largely from Forest, Grassland and Sparse vegetation (Fig. S1).

3.3. Consistency of future soil moisture trend

In Fig. 4, the mean value of Hurst exponent of global soil moisture is 0.71 with Hurst over 0.5 accounting for 87.69%. Thus, for the majority of the global land, the SM change trends during the study period have persistence in the future. Combining Hurst exponent with Theil-Sen slope, the proportion of the areas with SM persistently decreasing is 59.33%, remarkably larger than that (28.36%) of areas with SM persistently increasing, indicating that the global surface soil will keep drying for a certain period in the future; meanwhile, 10.4% of study area, such as central Australia, will perform an inverse SM trend. Fig. 4b shows the coupling information of the grades and future persistence of SM change. Specifically, the largest proportions of the areas with persistent and no change and persistent and strong decrease are 30.92% and 30.55%, respectively, followed by persistent and strong increase (10.68%) and persistent and slight decrease (10.54%); the areas with anti-persistent change account for 8.08%, mainly located in the central Siberian Plateau, Oceania and so on, manifesting that the SM trend in these areas will fluctuate in the future. The areas with anti-persistent and decrease, anti-persistent and slight decrease, anti-persistent and increase, and anti-persistent and slight increase account for 0.85%, 1.08%, 0.28%, and 0.11% respectively and their spatial distributions are scattered.

4. Discussion

4.1. Trend analysis based on EEMD and V statistic

This study adopted EEMD to decompose the time series of the global annual average SM from 1979 to 2017 and obtained four intrinsic mode functions (IMFs1–4) and its residual term. In Fig. 5, the global SM has average variation cycles of 3.25 yr (IMF1) and 7.8 yr (IMF2) on the interannual scale and 18.5 yr (IMF3) on the interdecadal scale. The average period of IMF4 is uncertain due to the limitation of temporal length. The residual component representing the general trend of the original signal showed a decreasing trend from 1979 to 2017. The contribution of components from EEMD to the original data can be evaluated by the variance contribution rate. It is found that the residual

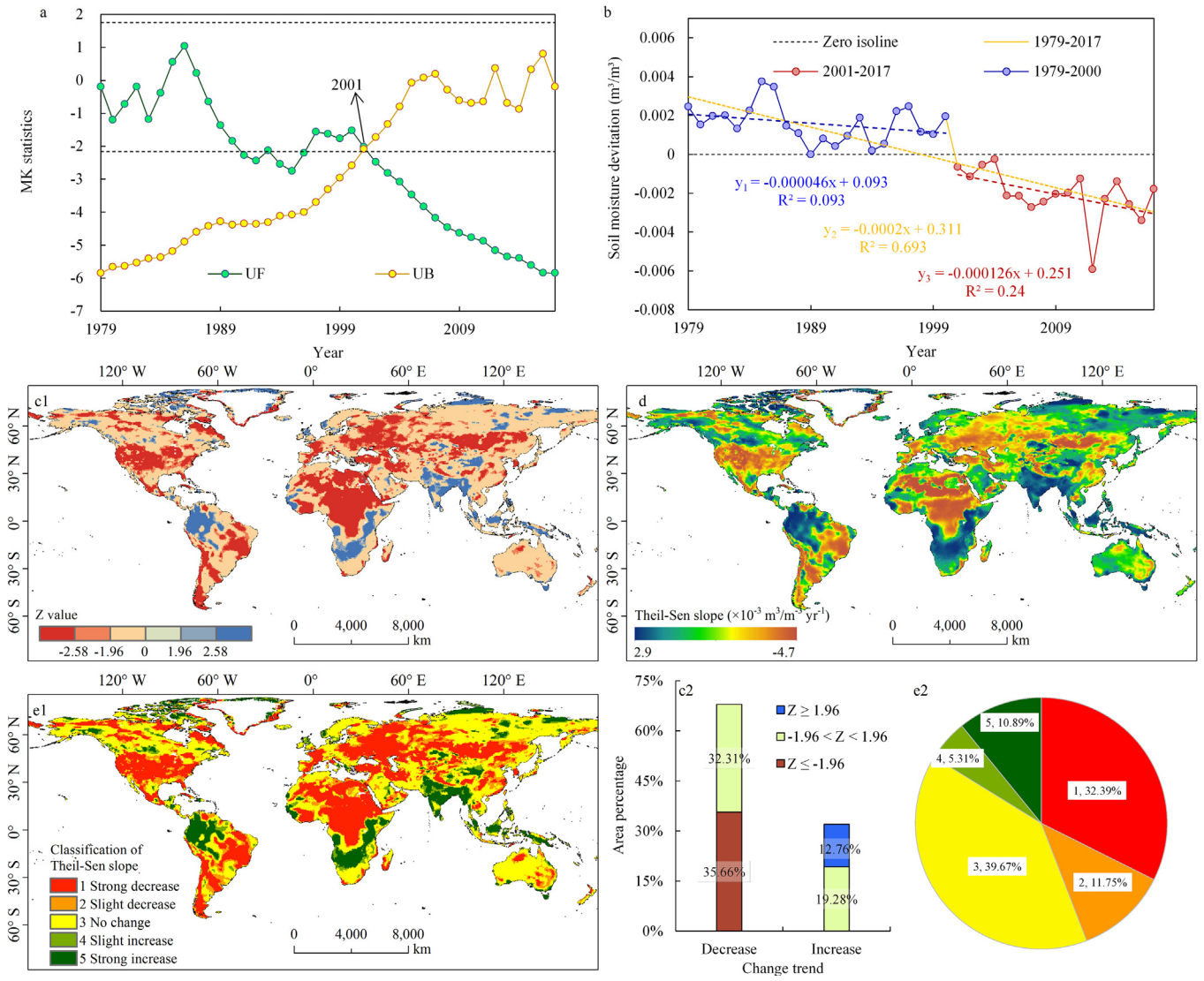

Fig. 2. Trend characteristics of SM from 1979 to 2017 at the global average scale and the pixel scale. Fig. 2a-b shows the MK test and the linear trends for global average SM anomalies; $y_{1\text{-}3}$ in Fig. 2b are regression equations for 1979–2000, 1979–2017, and 2001–2017, respectively; Fig. 2c1-2 shows the spatial distribution and its statistics of the MK test; Fig. 2d and 2e1 are spatial distributions of Theil-Sen slope and its re-classification and Fig. 2e2 is the area statistic of Fig. 2e1.

has the maximum variance, about 38.19%, and the variance contribution rates of IMFs1–4 are 24.19%, 16.77%, 18.63%, and 2.22%, respectively.

Fig. 6 shows that Hurst exponents of the global average original SM series and the residual term of EEMD decomposition are identical; they are 0.9707 and 0.989, respectively. Thus, the trend of the global average SM has very strong persistence. However, several inflection points exist in the V statistic of the original sequence in Fig. 6a. The first inflection point reveals that the SM trend of the study period can last for four years in the future, while the V statistic of the EEMD residue has no inflection point in Fig. 6b, i.e., the stable trend of change will last for at least 39 years in the future. In summary, the global SM will keep a steady decreasing trend in the next four years and then still decrease overall but there will be fluctuations in varying degrees.

4.2. Causes of soil drying and wetting trends

To clarify the effects of precipitation, temperature, and NDVI on SM, partial correlation was conducted at the pixel scale. The partial correlation coefficients (R_p) between three influencing factors and SM in Fig. 7 show that SM mainly positively correlates with precipitation and the R_p values range from −0.64 to 0.92. SM largely negatively correlates with temperature and R_p values vary from −0.89 to 0.81; spatially, their positive (negative) correlation areas have good consistency with the spatial distributions of soil wetting (drying) across the globe. The R_p values between SM and NDVI are from −0.86 to 0.85 with the area ratio between positive and negative correlation about 6:4. The positive correlation is distributed in South Asia, southern Africa, and other areas with soil wetting, and is also partly located in northern Europe and other areas with soil drying. The negative correlation is distributed in the north of Africa and other soil drying areas; also, it is fragmentarily distributed in the east of Russia and other soil wetting areas. The results reflect the double-sided effect of vegetation on SM. The maximum of absolute partial correlation coefficient (the strongest correlation) can potentially reveal the relative action intensity of three factors on SM change. The strongest correlation coefficients in Fig. 7d demonstrate that precipitation may play a dominant role in global SM change at the pixel scale with the area ratio between precipitation, temperature, and NDVI about 27:13:10.

The absolute value of the maximum partial correlation coefficient can distinguish the effect degree of each factor on SM. However, it has masked the situation that the partial correlation coefficients between influencing factors and SM are close, that is, the change of SM is possibly affected by the coupling of precipitation, temperature, and NDVI.

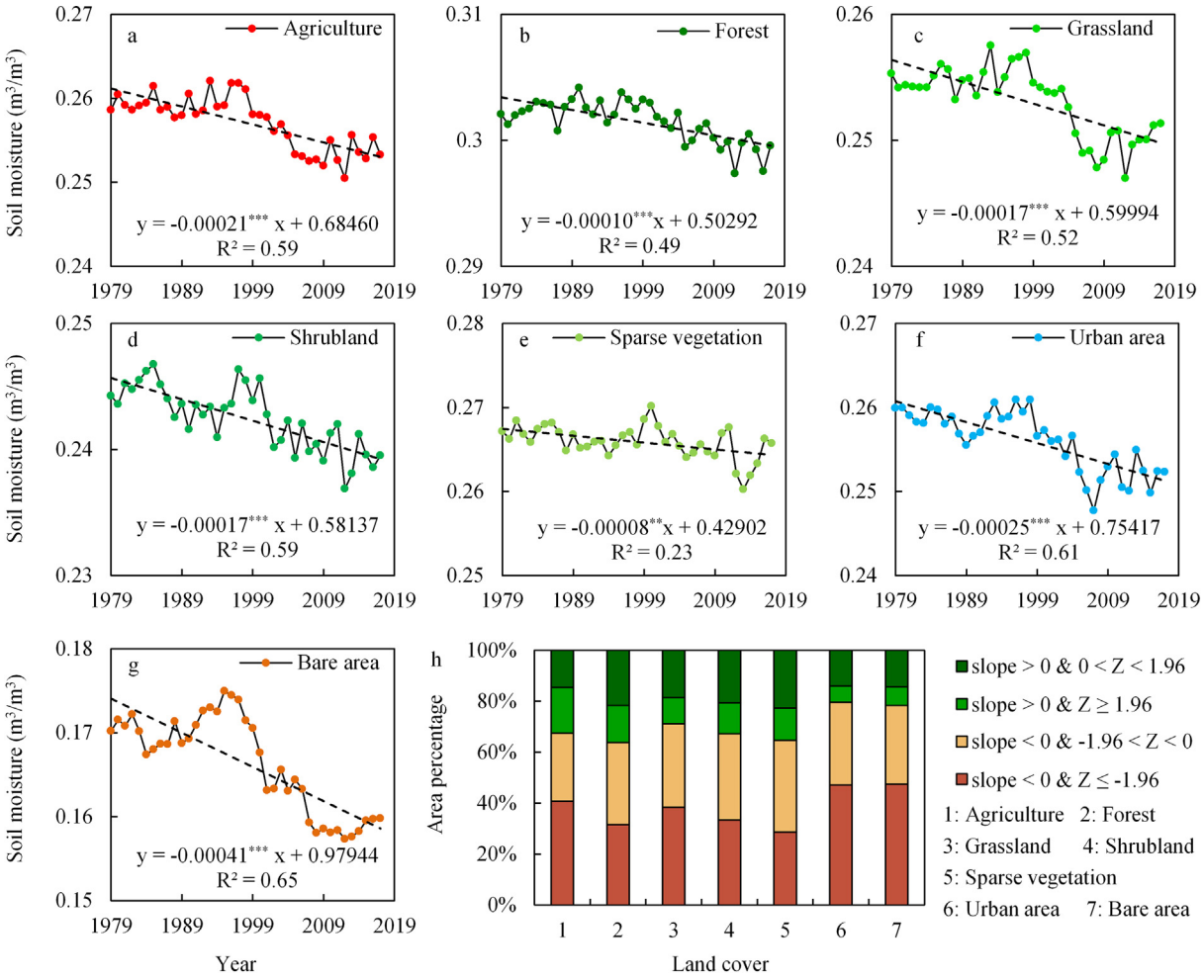

Fig. 3. SM trends (a-g) and the area statistics of Theil-Sen slope (h) under different land cover types in 1979–2017. Fig. 3h shows the area percentage of Theil-Sen slope based on the Z value of the MK test for each land cover. *, **, *** indicate significance at *P* value ≤ 0.05, *P* value ≤ 0.01, *P* value ≤ 0.001, respectively.

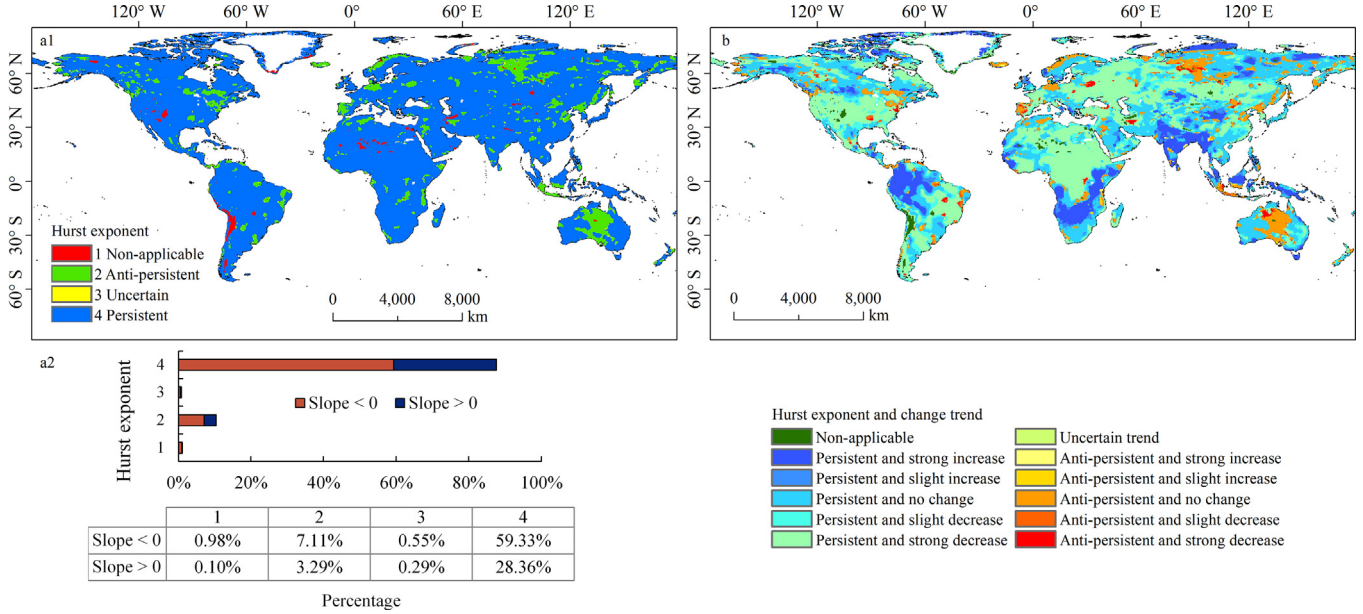

	1	2	3	4
Slope < 0	0.98%	7.11%	0.55%	59.33%
Slope > 0	0.10%	3.29%	0.29%	28.36%

Fig. 4. Future persistence of SM trend from 1979 to 2017. Fig. 4a1-2 is the spatial distribution for Hurst exponent of SM and its statistical results; Fig. 4b is the re-classified spatial distribution obtained by overlaying Hurst exponent and Theil-Sen slope grade maps.

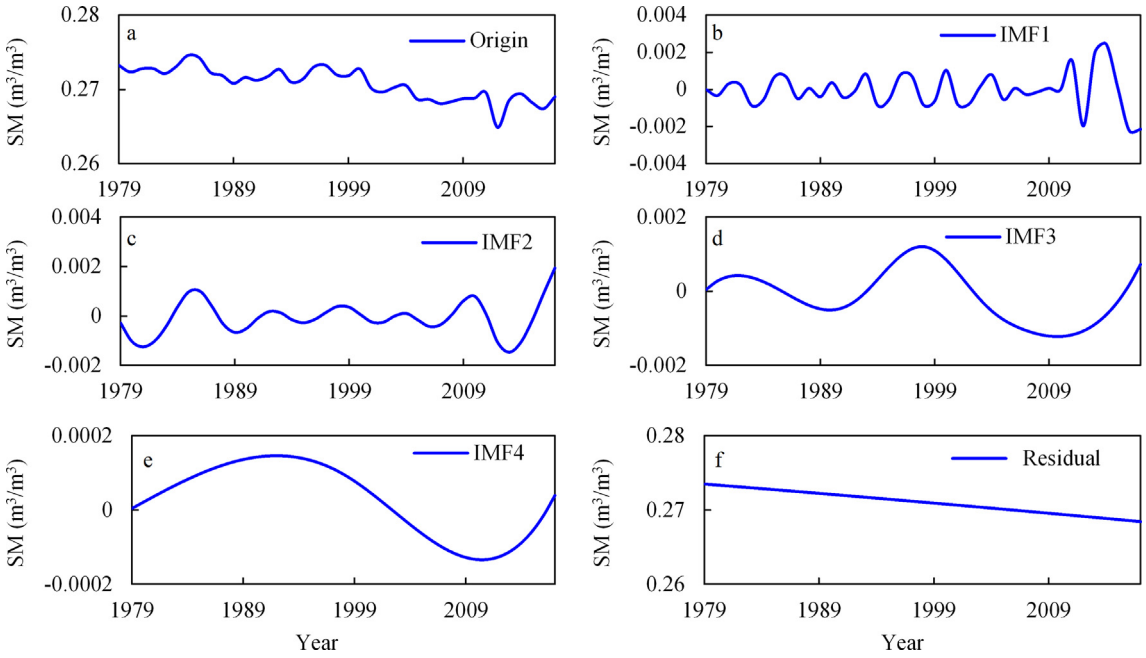

Fig. 5. IMF components and the residual of the global average SM from 1979 to 2017. In Fig. 5, SM means soil moisture.

Furthermore, it just reflects the relationship on the pixel (local) scale. Consequently, the causes of soil drying and wetting trends were studied at the global/regional average scale. Before that, the time series of global/regional average precipitation, temperature, NDVI, and SM were standardized by their standard deviations. For the whole research area, global soil-drying areas and soil-wetting areas, the annual precipitation, the annual average temperature, and NDVI increased significantly from 1982 to 2015 and the change rate of precipitation in global soil-drying areas is more than three times that in global soil-wetting areas (Fig. S2).

In Table 2, the change of global average SM is significantly negatively correlated with temperature, which is consistent with the conclusion of Cheng and Huang (2016). More importantly, temperature is the chief factor for the overall trend of global average SM with the explanatory power of 53.8%. It may be that the increase in soil evaporation and vegetation transpiration induced by the rising in temperature exceeds the supply from precipitation and ultimately leads to global soil drying. According to the result of Oki and Kanae (2006), evapotranspiration returns 60% of the total precipitation to the atmosphere. The average SM change of global soil-drying areas also has a significant negative correlation with temperature, and the stepwise regression shows that the trend of soil drying is mainly affected by the increase of temperature with the explanatory power of 65.1%. In the global soil-wetting areas, SM is significantly positively correlated with precipitation, temperature, and vegetation, but the correlation with precipitation is the strongest, followed by temperature and NDVI. Nevertheless, the results show that the increase of SM is caused by the combination of the increase of precipitation, temperature, and vegetation, and their influence on SM is similar according to the standardized coefficients with the combined explanatory power over 80%.

4.3. Impacts of soil drying trend

Across the globe, areas, where the annual average SM is lower than their multi-year average, were expanding at a rate of 1% per year in 1979–2017 (Fig. S3). Based on the global population density data with

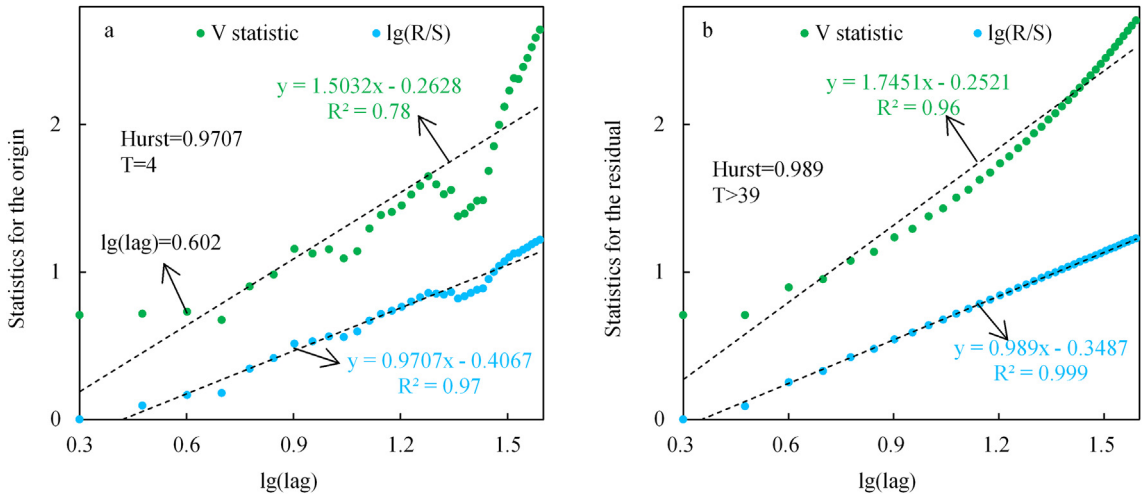

Fig. 6. Hurst exponents and its V statistics for the original global average SM (a) and the residual term of EEMD (b). In Fig. 6, the unit of lag is yr and T is the average cycle length of the system.

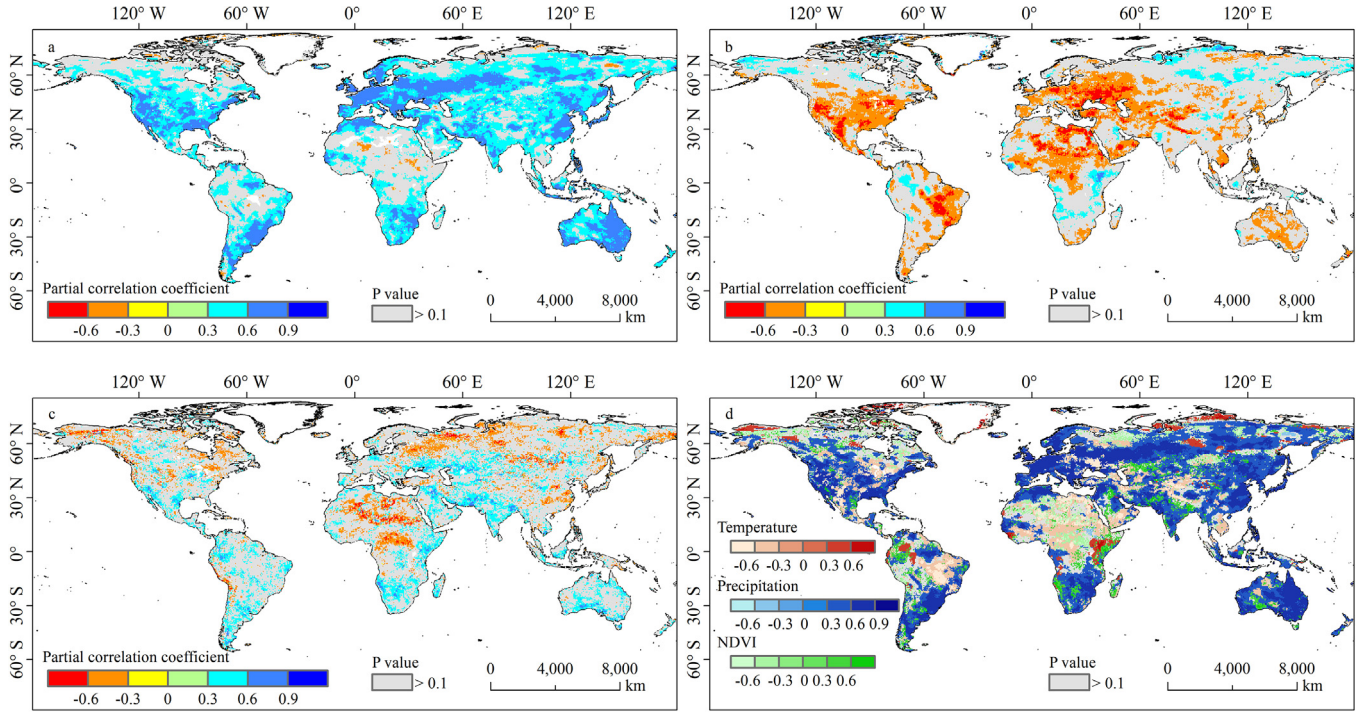

Fig. 7. Partial correlation coefficients between annual precipitation, annual average temperature, annual average NDVI, and SM in 1982–2015 (a-c) and the strongest partial correlation coefficient (d).

a five-year temporal resolution (Center for International Earth Science Information Network (CIESIN), Columbia University, 2017), we find that potential populations affected by soil drying have grown significantly, and the spatial distribution can be found in Fig. S4. Hurst exponent indicates that the global SM will decrease persistently in the future. It is supported by the results of Feng and Fu (2013) that the global arid areas have expanded in the past 60 years and will continue to increase in the 21st century. Also, Dai (2013) proposed that under global warming, drought areas in many lands would expand.

The dynamic changes of SM affect soil ecological environment (Zhang et al., 2013). Under drying conditions, the depth of soil water exchange decreases, and the regulating capacity of soil reservoirs is weakened; in water-restricted areas, such as the Loess Plateau of China, the perennial SM shortage has generated soil drying layer (Wang et al., 2010); additionally, soil organic carbon will be physically broken and mineralized (Achat et al., 2012), thereby increasing the loss of wetland organic carbon (Chen et al., 2018b), and soil microbial respiration rate will decrease (Manzoni and Katul, 2014). Bad soil conditions can lead to soil quality degeneration and ecosystem degradation (Shangguan, 2007; Whitmore and Whalley, 2009; Huber et al., 2011; Wang et al., 2018a). And, soil drying can result in frequent agricultural droughts and food security problems. According to crop maps in the study of Urban et al. (2017), SM in the United States, Southern Europe, Northern China, and South America, which are the primary producers of maize and wheat in the world, decreased in 1979–2017. Furthermore, soil drying may reduce or even exceed the potential benefits of rising temperature on photosynthesis in seasonally cold regions (Seo et al., 2019). For climate, when SM becomes dry, soil evaporation reduces and then precipitation generally decreases (Cheruy et al., 2017) due to less water vapor. Alonge et al. (2007) proposed that soil drying in the Sahel of West Africa resulted in a 55% reduction in precipitation. In energy balance, the decrease in SM makes latent heat reduce and sensible heat increase, and then temperature rises. Previous studies have revealed that SM drying can exert an important impact on heatwaves and extremely high temperature in large-scale areas, such as the extreme heat wave events in Europe in 2003 and Russia in 2010 (Della-Marta et al., 2007; Weisheimer et al., 2011). Under the conditions of global temperature rising and population growing, the decreasing trend of global SM will further lead to more population exposed to extreme heatwaves, land degradation, and other harsh environments.

5. Conclusions

Using ETC method, SM products from various sources were evaluated. Then, Theil-Sen estimate, EEMD, and other methods were used to reveal the trend of SM change at global average and pixel scales, and the trend of SM change after the study period was predicted by Hurst exponent. Finally, the reasons for SM change were analyzed by using partial correlation and stepwise regression. The conclusions are as follows:

Table 2
Partial correlation and stepwise regression of global/regional average soil moisture with time series of annual precipitation, annual average temperature, and annual average NDVI from 1982 to 2015. The soil drying (wetting) areas are places where Theil-Sen slopes are under (over) zero in Fig. 2d. Significant mark of partial correlation coefficient: '***', 0.001.

Factors	Partial correlation coefficient			Stepwise regression		
	Global	Soil drying	Soil wetting	Global	Soil drying	Soil wetting
Precipitation (x_1)	−0.12	−0.11	0.61^{***}	$y = -0.734x_2$, $R^2 = 0.538$	$y = -0.807x_2$, $R^2 = 0.651$	$y = 0.374x_1 + 0.374x_2 + 0.364x_3$ $R^2 = 0.82$
Temperature (x_2)	-0.65^{***}	-0.74^{***}	0.56^{***}			
NDVI (x_3)	0.16	0.20	0.54^{***}			

(1) ERA-Interim SM reflects the change of the true value best with the global average correlation coefficient of 0.748 and average RMSE of 0.021 m^3/m^3, followed by ESA CCI product, while SM product from GLDAS performs the worst.
(2) The global average SM experienced a significant drying trend in 1979–2017 and the trend accelerated in 2001–2017. In space, soil in 67.96% (32.39%, Sig.) of the globe covered with SM data, including Europe and central Africa, was drying.
(3) Overall, SM under land cover types declined in the study period. SM in Bare area decreased fastest with the rate of -0.41×10^{-3} m^3/m^3 yr^{-1}, whereas SM in Sparse vegetation decreased slowest with its rate of -0.08×10^{-3} m^3/m^3 yr^{-1}.
(4) With the global average Hurst exponent of SM over 0.7 and 59.33% of the global SM persistently drying, and the global SM change will be dominated by a decreasing trend in the next years.
(5) The trend of SM reduction is mainly induced by the rising of temperature with the explanation power over 60%, while soil wetting is caused by the interaction of temperature, precipitation, and NDVI with the explanation power of 82%.
(6) Under global warming, the global soil drying area in 1979–2017 increased rapidly at the rate of 1% yr^{-1}, and this trend will continue in the future.

In this study, ETC was not applied to every location in the world due to objective factors, possibly affecting the reliability of three soil moisture products. However, literature has verified that these products used in our study perform well among the existing products; moreover, the areas verified by ETC cover different land types, altitudes, and latitudes. Therefore, the results of this study are reliable and can provide a theoretical basis for the dynamic change of soil moisture and respective applications in soil hydrology, climate prediction, agricultural drought, and other fields.

6. Data availability statement

The fundamental data used in our study is available in the public, and their websites are provided in the "**2 Materials and methods**" section and other data are available from the corresponding author upon reasonable request.

7. Declarations of interest

None

Author contributions section

Shijie Wang and Xiaoyong Bai conceived the idea; Guangjie Luo, Luhua Wu, Chaojun Li, Yujie Yang, Zeyin Hu and Shiqi Tian provided comments and suggestions regarding the manuscript. Yue Cao and Huiwen Li provided technical guidance for data processing. Yuanhong Deng prepared materials, analyzed the results and wrote the article. All authors contributed to revision and reviewed the manuscript.

Acknowledgments

We thank the ESA (http://www.esa-cci.org/), NASA (https://disc.gsfc.nasa.gov/) and ECMWF (https://www.ecmwf.int/) for sharing SM products freely, and thank the ESA CCI Land Cover Project for providing land cover map. The research was supported by the Strategic Priority Research Program of the Chinese Academy of Sciences [grant number XDA23060100], National Key Research Program of China [grant numbers 2016YFC0502300 & 2016YFC0502102), Western Light Talent Program (Category A) [grant number 2018-99], United fund of Karst Science Research Center [grant number U1612441], Science and Technology Plan of Guizhou Province of China [grant number 2017–2966].

Appendix A. Supplementary data

Supplementary data to this article can be found online at https://doi.org/10.1016/j.ecolind.2019.105939.

References

Achat, D.L., Augusto, L., Gallet-Budynek, A., Bakker, M.R., 2012. Drying-induced changes in phosphorus status of soils with contrasting soil organic matter contents - implications for laboratory approaches. Geoderma 187, 41–48.
Albergel, C., de Rosnay, P., Balsamo, G., Isaksen, L., Munoz-Sabater, J., 2012a. Soil Moisture Analyses at ECMWF: Evaluation Using Global Ground-Based In Situ Observations. J. Hydrometeorol. 13, 1442–1460.
Albergel, C., de Rosnay, P., Gruhier, C., Munoz-Sabater, J., Hasenauer, S., Isaksen, L., Kerr, Y., Wagner, W., 2012b. Evaluation of remotely sensed and modelled soil moisture products using global ground-based in situ observations. Remote Sens. Environ. 118, 215–226.
Albergel, C., Dorigo, W., Reichle, R.H., Balsamo, G., de Rosnay, P., Munoz-Sabater, J., Isaksen, L., de Jeu, R., Wagner, W., 2013. Skill and Global Trend Analysis of Soil Moisture from Reanalyses and Microwave Remote Sensing. J. Hydrometeorol. 14, 1259–1277.
Alonge, C.J., Mohr, K.I., Tao, W.-K., 2007. Numerical studies of wet versus dry soil regimes in the West African Sahel. J. Hydrometeorol. 8, 102–116.
Berg, A.A., Famiglietti, J.S., Rodell, M., Reichle, R.H., Jambor, U., Holl, S.L., Houser, P.R., 2005. Development of a hydrometeorological forcing data set for global soil moisture estimation. Int. J. Climatol. 25, 1697–1714.
Brocca, L., Hasenauer, S., Lacava, T., Melone, F., Moramarco, T., Wagner, W., Dorigo, W., Matgen, P., Martinez-Fernandez, J., Llorens, P., Latron, J., Martin, C., Bittelli, M., 2011. Soil moisture estimation through ASCAT and AMSR-E sensors: an intercomparison and validation study across Europe. Remote Sens. Environ. 115, 3390–3408.
Cai, W., Cowan, T., Briggs, P., Raupach, M., 2009. Rising temperature depletes soil moisture and exacerbates severe drought conditions across southeast Australia. Geophys. Res. Lett., pp. 36.
Center for International Earth Science Information Network (CIESIN), Columbia University, 2017. Documentation for the Gridded Population of the World, Version 4 (GPWv4), Revision 10 Data Sets. Palisades NY: NASA Socioeconomic Data and Applications Center (SEDAC). https://doi.org/10.7927/H4B56GPT (accessed 10 July 2018).
Chen, F., Crow, W.T., Bindlish, R., Colliander, A., Burgin, M.S., Asanuma, J., Aida, K., 2018a. Global-scale evaluation of SMAP, SMOS and ASCAT soil moisture products using triple collocation. Remote Sens. Environ. 214, 1–13.
Chen, H., Zou, J., Cui, J., Nie, M., Fang, C., 2018b. Wetland drying increases the temperature sensitivity of soil respiration. Soil Biol. Biochem. 120, 24–27.
Chen, X., Zhang, Z., Chen, X., Shi, P., 2009. The impact of land use and land cover changes on soil moisture and hydraulic conductivity along the karst hillslopes of southwest China. Environ. Earth Sci. 59, 811–820.
Cheng, S., Huang, J., 2016. Enhanced soil moisture drying in transitional regions under a warming climate. J. Geophys. Res.-Atmos. 121, 2542–2555.
Cheruy, F., Dufresne, J.L., Mesbah, S.A., Grandpeix, J.Y., Wang, F., 2017. Role of Soil Thermal Inertia in Surface Temperature and Soil Moisture-Temperature Feedback. J. Adv. Model. Earth Sy. 9, 2906–2919.
Dai, A., 2013. Increasing drought under global warming in observations and models. Nat. Clim. Change 3, 52–58.
Dee, D.P., Uppala, S.M., Simmons, A.J., Berrisford, P., Poli, P., Kobayashi, S., Andrae, U., Balmaseda, M.A., Balsamo, G., Bauer, P., Bechtold, P., Beljaars, A.C.M., van de Berg, L., Bidlot, J., Bormann, N., Delsol, C., Dragani, R., Fuentes, M., Geer, A.J., Haimberger, L., Healy, S.B., Hersbach, H., Holm, E.V., Isaksen, L., Kallberg, P., Koehler, M., Matricardi, M., McNally, A.P., Monge-Sanz, B.M., Morcrette, J.J., Park, B.K., Peubey, C., de Rosnay, P., Tavolato, C., Thepaut, J.N., Vitart, F., 2011. The ERA-Interim reanalysis: configuration and performance of the data assimilation system. Q. J. Roy. Meteor. Soc. 137, 553–597.
Della-Marta, P.M., Luterbacher, J., von Weissenfluh, H., Xoplaki, E., Brunet, M., Wanner, H., 2007. Summer heat waves over western Europe 1880–2003, their relationship to large-scale forcings and predictability. Clim. Dynam. 29, 251–275.
Deng, Y., Wang, S., Bai, X., Luo, G., Wu, L., Chen, F., Wang, J., Li, Q., Li, C., Yang, Y., Hu, Z., Tian, S., 2019. Characteristics of soil moisture storage from 1979 to 2017 in the karst area of China. Geocarto Int.
Deng, Y., Wang, S., Bai, X., Wu, L., Cao, Y., Li, C., Li, H., Hu, Z., 2018. Relationship between soil moisture and climate and its memory in Southwest China. Acta Ecol. Sin. 38, 8688–8699.
Dorigo, W., de Jeu, R., Chung, D., Parinussa, R., Liu, Y., Wagner, W., Fernandez-Prieto, D., 2012. Evaluating global trends (1988–2010) in harmonized multi-satellite surface soil moisture. Geophys. Res. Lett., pp. 39.
Dorigo, W.A., Gruber, A., De Jeu, R.A.M., Wagner, W., Stacke, T., Loew, A., Albergel, C., Brocca, L., Chung, D., Parinussa, R.M., Kidd, R., 2015. Evaluation of the ESA CCI soil moisture product using ground-based observations. Remote Sens. Environ. 162, 380–395.
English, N.B., Weltzin, J.F., Fravolini, A., Thomas, L., Williams, D.G., 2005. The influence of soil texture and vegetation on soil moisture under rainout shelters in a semi-desert grassland. J. Arid Environ. 63, 324–343.
ESA: Land Cover CCI Product User Guide Version 2.0.7, available at: http://maps.elie.ucl.ac.be/CCI/viewer/download.php (access: 10 July 2018).
Feng, S., Fu, Q., 2013. Expansion of global drylands under a warming climate. Atmos.

Chem. Phys. 13, 10081–10094.
Fernandes, R., Leblanc, S.G., 2005. Parametric (modified least squares) and non-parametric (Theil-Sen) linear regressions for predicting biophysical parameters in the presence of measurement errors. Remote Sens. Environ. 95, 303–316.
Harris, I., Jones, P.D., Osborn, T.J., Lister, D.H., 2014. Updated high-resolution grids of monthly climatic observations - the CRU TS3.10 Dataset. Int. J. Climatol. 34, 623–642.
Huang, N.E., Shen, Z., Long, S.R., Wu, M.L.C., Shih, H.H., Zheng, Q.N., Yen, N.C., Tung, C.C., Liu, H.H., 1998. The empirical mode decomposition and the Hilbert spectrum for nonlinear and non-stationary time series analysis. P. Roy. Soc. A-Math. Phy. 454, 903–995.
Huber, S., Fensholt, R., Rasmussen, K., 2011. Water availability as the driver of vegetation dynamics in the African Sahel from 1982 to 2007. Global Planet. Change 76, 186–195.
Kim, H., Parinussa, R., Konings, A.G., Wagner, W., Cosh, M.H., Lakshmi, V., Zohaib, M., Choi, M., 2018. Global-scale assessment and combination of SMAP with ASCAT (active) and AMSR2 (passive) soil moisture products. Remote Sens. Environ. 204, 260–275.
Koster, R.D., Suarez, M.J., Higgins, R.W., Van den Dool, H.M., 2003. Observational evidence that soil moisture variations affect precipitation. Geophys. Res. Lett., pp. 30.
Legates, D.R., Mahmood, R., Levia, D.F., DeLiberty, T.L., Quiring, S.M., Houser, C., Nelson, F.E., 2011. Soil moisture: A central and unifying theme in physical geography. Prog. Phys. Geogr. 35, 65–86.
Li, W., MacBean, N., Ciais, P., Defourny, P., Lamarche, C., Bontemps, S., Houghton, R.A., Peng, S., 2018. Gross and net land cover changes in the main plant functional types derived from the annual ESA CCI land cover maps (1992–2015). Earth Syst. Sci. Data 10, 219–234.
Li, Y., 2001. Effects of forest on water circle on the Loess Plateau. Journal of Natural Resources. 16, 427–432.
Manzoni, S., Katul, G., 2014. Invariant soil water potential at zero microbial respiration explained by hydrological discontinuity in dry soils. Geophys. Res. Lett. 41, 7151–7158.
McColl, K.A., Alemohammad, S.H., Akbar, R., Konings, A.G., Yueh, S., Entekhabi, D., 2017. The global distribution and dynamics of surface soil moisture. Nat. Geosci. 10, 100-+.
McColl, K.A., Vogelzang, J., Konings, A.G., Entekhabi, D., Piles, M., Stoffelen, A., 2014. Extended triple collocation: Estimating errors and correlation coefficients with respect to an unknown target. Geophys. Res. Lett. 41, 6229–6236.
Oki, T., Kanae, S., 2006. Global hydrological cycles and world water resources. Science 313, 1068–1072.
Padilla, F.M., Pugnaire, F.I., 2007. Rooting depth and soil moisture control Mediterranean woody seedling survival during drought. Funct. Ecol. 21, 489–495.
Qin, Z., Zou, X., Weng, F., 2012. Comparison between linear and nonlinear trends in NOAA-15 AMSU-A brightness temperatures during 1998–2010. Clim. Dynam. 39, 1763–1779.
Rodell, M., Houser, P.R., Jambor, U., Gottschalck, J., Mitchell, K., Meng, C.J., Arsenault, K., Cosgrove, B., Radakovich, J., Bosilovich, M., Entin, J.K., Walker, J.P., Lohmann, D., Toll, D., 2004. The global land data assimilation system. B. Am. Meteorol. Soc. 85, 381-+.
Rodriguez-Fonseca, B., Mohino, E., Mechoso, C.R., Caminade, C., Biasutti, M., Gaetani, M., Garcia-Serrano, J., Vizy, E.K., Cook, K., Xue, Y., Polo, I., Losada, T., Druyan, L., Fontaine, B., Bader, J., Doblas-Reyes, F.J., Goddard, L., Janicot, S., Arribas, A., Lau, W., Colman, A., Vellinga, M., Rowell, D.P., Kucharski, F., Voldoire, A., 2015. Variability and Predictability of West African Droughts: A Review on the Role of Sea Surface Temperature Anomalies. J. Climate 28, 4034–4060.
Scipal, K., Dorigo, W., Dejeu, R., 2010. Triple collocation — A new tool to determine the error structure of global soil moisture products. Geoscience Remote Sensing Symposium.
Scipal, K., Holmes, T., de Jeu, R., Naeimi, V., Wagner, W., 2008. A possible solution for the problem of estimating the error structure of global soil moisture data sets. Geophys. Res. Lett., pp. 35.
Sen, P.K., 1968. Estimates of the regression coefficient based on Kendall's tau. J. Am. Stat. Assoc. 63 (324), 1379-+.
Seo, E., Lee, M.-I., Jeong, J.-H., Koster, R.D., Schubert, S.D., Kim, H.-M., Kim, D., Kang, H.-S., Kim, H.-K., MacLachlan, C., Scaife, A.A., 2019. Impact of soil moisture initialization on boreal summer subseasonal forecasts: mid-latitude surface air temperature and heat wave events. Clim. Dynam. 52, 1695–1709.
Shangguan, Z.P., 2007. Soil desiccation occurrence an its impact on forest vegetation in the Loess Plateau of China. Int. J. Sust. Dev. World 14, 299–306.
Sheffield, J., Wood, E.F., 2008. Global trends and variability in soil moisture and drought characteristics, 1950–2000, from observation-driven Simulations of the terrestrial hydrologic cycle. J. Climate 21, 432–458.
Su, C.-H., Ryu, D., Crow, W.T., Western, A.W., 2014. Beyond triple collocation: Applications to soil moisture monitoring. J. Geophys. Res.-Atmos. 119, 6419–6439.
Taylor, C.M., de Jeu, R.A.M., Guichard, F., Harris, P.P., Dorigo, W.A., 2012. Afternoon rain more likely over drier soils. Nature 489, 423–426.
Tian, F., Fensholt, R., Verbesselt, J., Grogan, K., Horion, S., Wang, Y., 2015. Evaluating temporal consistency of long-term global NDVI datasets for trend analysis. Remote Sens. Environ. 163, 326–340.
Urban, D.W., Sheffield, J., Lobell, D.B., 2017. Historical effects of CO_2 and climate trends on global crop water demand. Nat. Clim. Change 7, 901-+.
Valdes, J.B., Seoane, R.S., North, G.R., 2015. A methodology for the evaluation of global warming impact on soil-moisture and runoff. J. Hydrol. 161, 389–413.
Wang, S., Fu, B., Gao, G., Liu, Y., Zhou, J., 2013. Responses of soil moisture in different land cover types to rainfall events in a re-vegetation catchment area of the Loess Plateau, China. Catena 101, 122–128.
Wang, X., Wang, B., Xu, X., Liu, T., Duan, Y., Zhao, Y., 2018. Spatial and temporal variations in surface soil moisture and vegetation cover in the Loess Plateau from 2000 to 2015. Ecol. Indic. 95, 320–330.
Wang, Y., Shao, M.A., Liu, Z., 2010. Large-scale spatial variability of dried soil layers and related factors across the entire Loess Plateau of China. Geoderma 159, 99–108.
Wang, Y., Shao, M.A., Zhu, Y., Sun, H., Fang, L., 2018. A new index to quantify dried soil layers in water-limited ecosystems: a case study on the Chinese Loess Plateau. Geoderma 322, 1–11.
Weisheimer, A., Doblas-Reyes, F.J., Jung, T., Palmer, T.N., 2011. On the predictability of the extreme summer 2003 over Europe. Geophys. Res. Lett., pp. 38.
Whitmore, A.P., Whalley, W.R., 2009. Physical effects of soil drying on roots and crop growth. J. Exp. Bot. 60, 2845–2857.
Wu, L., Wang, S., Bai, X., Luo, W., Tian, Y., Zeng, C., Luo, G., He, S., 2017. Quantitative assessment of the impacts of climate change and human activities on runoff change in a typical karst watershed. SW China. Sci. Total Environ. 601, 1449–1465.
Wu, W.R., Geller, M.A., Dickinson, R.E., 2002. The response of soil moisture to long-term variability of precipitation. J. Hydrometeorol. 3, 604–613.
Yue, S., Pilon, P., Cavadias, G., 2002. Power of the Mann-Kendall and Spearman's rho tests for detecting monotonic trends in hydrological series. J. Hydrol. 259, 254–271.
Zeng, J., Li, Z., Chen, Q., Bi, H., Qiu, J., Zou, P., 2015. Evaluation of remotely sensed and reanalysis soil moisture products over the Tibetan Plateau using in-situ observations. Remote Sens. Environ. 163, 91–110.
Zhang, J., Wang, W.-C., Wei, J., 2008. Assessing land-atmosphere coupling using soil moisture from the Global Land Data Assimilation System and observational precipitation. J. Geophys. Res.-Atmos, 113.
Zhang, S., Yang, H., Yang, D., Jayawardena, A.W., 2016. Quantifying the effect of vegetation change on the regional water balance within the Budyko framework. Geophys. Res. Lett. 43, 1140–1148.
Zhang, X.F., Zhao, L., Xu Jr., S.J., Liu, Y.Z., Liu, H.Y., Cheng, G.D., 2013. Soil moisture effect on bacterial and fungal community in Beilu River (Tibetan Plateau) permafrost soils with different vegetation types. J. Appl. Microbiol. 114, 1054–1065.